南京航空航天大学

论文集

（二〇〇二年）

第9册

四院

南京航空航天大学科技部编

二〇〇二年六月

四　　院

○四一系

序号	姓　名	职称	单位	论文题目	刊物、会议名称	年、卷、期	类别
1	包骅 周建江 葛志雄 曹建华 夏伟杰	硕士 正高 硕士 硕士 硕士	041 041 041 041 041	Digital Phase Detecting Based On Transform and Its DSP Implementation	2002年东北亚信息技术研讨会	2002.01	
2	陈吉忠 方琰崴	副高 硕士	041 041	低峰值平均功率比的多载波CDMA	通信技术	2002.00.10	J
3	程堂柏 周建江 虞震东 舒永泽	博士 正高 博士 正高	041 041 041 041	Analysis of the FMM Electromagnetic Scattering of Multiple Conducting Cylinder	IEEE Anternas and Propagation Society International Symposium and USNC/URSI	2002.01	
4	程堂柏 周建江 虞震东 舒永泽	博士 正高 博士 正高	041 041 041 041	多个散射体散射分析的RATMA法	南京师范大学学报	2002.2.03	J
5	程堂柏 周建江 虞震东 舒永泽	博士 正高 博士 正高	041 041 041 041	多导体柱电磁散射的快速算法	上海大学学报自然科学版	2002.8.05	H
6	程堂柏 周建江 虞震东 舒永泽	博士 正高 博士 正高	041 041 041 041	窗函数递推T矩阵法分析柱体的散射	全国电磁兼容会议	2002.01	
7	丁卫平	博士	041	背腔式微带天线电磁散射分析的FEM?PTD方法	电波科学学报	2002.17.04	
8	丁卫平 徐金平	博士 正高	041 041	带有腔体式槽缝的电大尺寸目标电磁散射特性分析	电子学报	2002.30.06	EI、H
9	郭春生 朱兆达 朱岱寅 张弓	博士 正高 中级 副高	041 041 041 041	一种新的基于形态学的InSAR干涉相位图滤波算法	数据采集与处理	2002.17.03	H
10	何小祥	博士	041	应用DDM/FEM方法研究开口腔体电磁散射特性	东南大学学报	2002.32.04	H
11	华夷和	博士	041	磁场积分方程矩量法中基函数的立体角终止	微波学报	2002.18.04	J
12	华夷和 徐金平 顾长青	博士 正高 正高	041 041 041	金属载体上线天线阻抗与辐射特性的矩量法研究	南京航空航天大学学报	2002.34.03	J
13	靖晟 刘渝 席轶敏	硕士 正高 硕士	041 041 041	非线性调频信号参数估计算法	南京航空航天大学学报	2001.33.05	J
14	廖闻剑 成瑜	博士 正高	041 041	一种基于笔划宽度的印鉴分割方法	数据采集与处理	2002.17.03	H
15	廖闻剑 成瑜	博士 正高	041 041	基于多分类器决策融合的印鉴真伪鉴别方法	南京航空航天大学学报	2002.34.04	J
16	刘渝 靖晟 席轶敏	正高 硕士 硕士	041 041 041	宽带欠采样信号处理解模糊方法	数据采集与处理	2001.16.03	H

序号	姓 名	职称	单位	论文题目	刊物、会议名称	年、卷、期	类别
17	沈绍清 吴宁	硕士 正高	041 041	A New symmetric Extension of the signal at the Boundaries for Multiwavelet Image Compression	6th International conference on Signal Processing	2002.01	
18	宋茂忠 许宗泽	正高 正高	041 041	圆天线阵时空调制扩频通信定位系统设计与仿真	厦门大学学报（自然科学版）	2002.41.01	H
19	宋茂忠	正高	041	一种新颖的四进制八相时空调制通信综合化系统	东南大学学报（自然科学版）	2002.32.01	EI、H
20	宋茂忠 许宗泽	正高 正高	041 041	一种新型八相时空调制扩频通信定位综合系统	应用科学学报	2002.20.04	H
21	谭姝 宋茂忠	硕士 正高	041 041	利用RCM2200实现以太网与异步串口之间的通信	计算机与信息技术	2002.00.10	
22	王成华 蒋爱民 吕勇	正高 硕士 硕士	041 041 041	可编程模拟器件的应用研究	数据采集与处理	2002.17.03	H
23	吴宁 段惠明 金杰	正高 其他1 硕士	041 外 041	电网监测系统中数据网关的实现	电力系统自动化	2002.26.24	H
24	武昕伟 朱兆达	博士 正高	041 041	基于聚束照射SAR成像算法的条带SAR数据处理	南京航空航天大学学报	2002.34.05	J
25	武昕伟 朱兆达	博士 正高	041 041	利用对比度最大化实现SAR图形自聚焦	现代雷达	2002.24.03	J
26	武昕伟 朱兆达 朱岱寅	博士 正高 中级	041 041 041	相位梯度自聚焦算法载条带模式SAR中的应用	数据采集与处理	2002.17.04	H
27	席轶敏 刘渝 靖晟	硕士 正高 硕士	041 041 041	电子侦察信号实时检测算法及性能分析	南京航空航天大学学报	2001.33.03	J
28	辛雅明 顾长青	硕士 正高	041 041	FDTD法计算铁氧体微带天线的RCS	电子与信息学报	2002.24.10	H
29	徐大专 樊迅 潘雄	正高 硕士 硕士	041 041 041	虚拟超声波探伤仪关键技术研究	无损检测	2002.24.04	J
30	颜彪 许宗泽	博士 正高	041 041	一种手提软件无线电终端体系结构的研究	通信技术	2002.00.06	J
31	颜彪 许宗泽	博士 正高	041 041	串行MSK DS/SSMA 系统性能分析	航空电子技术	2002.33.03	H
32	颜彪 许宗泽	博士 正高	041 041	一种新的抗转发干扰直接序列扩频系统的性能分析	数据采集与处理	2002.17.04	H
33	姚玉花 成瑜	硕士 正高	041 041	一种身份证扫描图像的二值化方法	机械制造与自动化	2002.00.05	

序号	姓 名	职称	单位	论文题目	刊物、会议名称	年、卷、期	类别
34	叶少华 朱兆达 朱岱寅	博士 正高 中级	041 041 041	一种改进的多通道干涉SAR/GMTI方案	电子与信息学报	2002.24.12	H
35	叶少华 朱兆达 朱岱寅	博士 正高 中级	041 041 041	一种改进的二端口杂波抑制干涉仪	系统工程与电子技术	2002.24.08	J
36	张弓 张桂芝	副高 副高	041 041	通信电子线路课程教学改革思路与探索	南京航空航天大学学报社科版	2002.4.00	
37	张弓 朱兆达	副高 正高	041 041	一种简捷的机载PD雷达杂波仿真算法研究	雷达与对抗	2002.00.03	
38	张弓 张景涛	副高 硕士	041 041	HPI主机接口在多处理器系统中的应用	电子技术应用	2002.28.07	J
39	张弓 朱兆达 吕波	副高 正高 硕士	041 041 041	多重滑窗算法在DSP上的并行实现	数据采集与处理	2002.17.02	H
40	张弓 朱兆达	副高 正高	041 041	Application of Fuzzy C-mean Cluster Algorithm on Clutter Tracking	Chinese Journal of Aeronautics	2002.15.01	EI、H
41	张景涛 张弓	硕士 副高	041 041	TMS320VC54系列EPROM的加载实现	国外电子元器件	2002.00.03	
42	张小飞	博士	041	超声检测中的噪声处理	无损检测	2002.24.05	J
43	张小飞 徐大专	博士 正高	041 041	虚拟式直接序列扩频通信电台的研究	电讯技术	2002.42.06	
44	张颖 吴宁	硕士 正高	041 041	基于VAI总线的多通道多采样率的数据采集系统	计算机测量与控制	2002.10.11	
45	张勇 刘渝	硕士 正高	041 041	多信号数字测向算法研究	数据采集与处理	2002.17.03	H
46	郑步生	中级	041	EWB在直流电动机混合仿真中的应用	机械制造与自动化	2002.00.06	
47	周建江 昂海松	正高 正高	041 011	An Analysis of Radar Targets Characteristics	2002年汉城航空大学50周年校庆学术会议	2002.01	
48	朱岱寅 朱兆达 谢求成	中级 正高 副高	041 041 121	一种基于局部频率估计的地形自适应干涉图滤波器	电子学报	2002.00.00	H
49	朱岱寅 Scheiber 沙南生 朱兆达	中级 其他1 副高 正高	041 外 外 041	An efficient adaptive filter for InSAR processing topography	High Technology Letters	2001.7.04	J
50	朱岱寅 朱兆达	中级 正高	041 041	机载 SAR斜视区域成像研究	电子学报	2002.30.09	H

FDTD 法计算铁氧体微带天线的 RCS [1]

辛雅明 顾长青

(南京航空航天大学信息科学与技术学院 南京 210016)

摘 要 该文采用并改进了一种将铁氧体进动方程直接离散的更有效的 FDTD 算法，在结合其它 FDTD 算法中的新技术基础上分析计算了任意方向外加偏置磁场时铁氧体矩形微带贴片天线的 RCS 频响特性并给出了一些有用的结论.

关键词 微带天线，时域有限差分法，雷达截面，铁氧体

中图号 TN826, TN817

1 引 言

早在 1953 年就有人提出了微带天线的概念，但是并未引起工程界的重视. 70 年代后由于微波集成技术的发展以及各种低耗介质材料的出现，微带天线的制作工艺得到了保证；而空间技术的发展，又迫切需要低剖面天线，因此新结构和高性能的微带天线不断涌现. 近年来，研究表明通过调整外加偏置磁场能够改变铁氧体微带天线的谐振频率达 40%[1]，也能改变天线的极化方向 [2] 以及减缩天线的峰值 RCS[3,4]，因此受到人们的极大关注. 文献 [3,4] 用谱域矩量法研究了铁氧体微带天线的 RCS，但是随着外加偏置磁场的方向改变，谱域格林函数的解析表达式要作相应地改变，推导过程过于繁琐，使其应用受到限制.

在磁化的铁氧体中，磁场强度和磁化强度的关系是通过 Gilbert 进动方程来描述的. 直接将进动方程和 Maxwell 方程进行差分离散得到铁氧体中的 FDTD 算法思想是文献 [5,6] 最早提出的. 之后 J. A. Pereda 提出了一种能在时间和空间上准确同步的铁氧体 FDTD 算法 [7]，算法中利用了循环的 Richtmyer 差分递推式，通过对电场强度矢量的空间内插来避开对磁感应强度矢量的内插. M. Okoniewski 提出了一种更为有效的铁氧体 FDTD 技术 [8]. 本文对文献 [8] 的方法作了进一步改进，在结合 FDTD 算法中的新技术基础上分析计算了任意方向外加偏置磁场时铁氧体矩形微带贴片天线的 RCS 的频响特性并给出了一些有用的结论.

2 理论分析

2.1 铁氧体中的 FDTD 算法

在饱和磁化的铁氧体中，电磁场由下面一组偏微分方程决定

$$\nabla \times \boldsymbol{E} = -\partial \boldsymbol{B}/\partial t \tag{1a}$$

$$\nabla \times \boldsymbol{H} = \partial \boldsymbol{D}/\partial t \tag{1b}$$

$$-\gamma(\boldsymbol{M} \times \boldsymbol{H}) = \partial \boldsymbol{M}/\partial t \tag{1c}$$

其中 γ 是旋磁比. 令 $\boldsymbol{M} = \boldsymbol{M}_0 + \boldsymbol{m}$，$\boldsymbol{H} = \boldsymbol{H}_0 + \boldsymbol{h}$，这里 $\boldsymbol{M}_0$，$\boldsymbol{H}_0$ 分别表示饱和磁化强度和外加偏置磁场，$\boldsymbol{m}$，$\boldsymbol{h}$ 表示时变的磁化强度和磁场强度. 在 $|\boldsymbol{M}_0| >> |\boldsymbol{m}|$，$|\boldsymbol{H}_0| >> |\boldsymbol{h}|$

[1] 2001-03-19 收到，2001-10-10 定稿
航空科学基金 97F52042 资助项目

的小信号条件下，考虑到 $\boldsymbol{B}=\mu_0(\boldsymbol{H}+\boldsymbol{M})$ 和 $\boldsymbol{D}=\varepsilon\boldsymbol{E}$ 本构关系，上式又可写成

$$\partial\boldsymbol{E}/\partial t=(1/\varepsilon)\nabla\times h \tag{2a}$$

$$\partial h/\partial t=-(1/\mu_0)\nabla\times\boldsymbol{E}-\partial\boldsymbol{m}/\partial t \tag{2b}$$

$$\partial\boldsymbol{m}/\partial t\approx-\gamma(\boldsymbol{m}\times\boldsymbol{H}_0+\boldsymbol{M}_0\times h) \tag{2c}$$

由于与外加偏置磁场方向垂直的平面上场分量是耦合的，因此 (2) 式在使用 Yee 氏中心差分法时需小心对待以维持中心差分递推式的二阶精度，即必须确保算法在时间上和空间上同步。

(2a) 和 (2b) 式的左边对时间的偏导离散有

$$(\boldsymbol{E}^n-\boldsymbol{E}^{n-1})/\Delta t=(1/\varepsilon)\{\nabla\times h\}^{n-1/2} \tag{3a}$$

$$(h^{n+1/2}-h^{n-1/2})/\Delta t=-(1/\mu_0)\{\nabla\times\boldsymbol{E}\}^n-\{\partial\boldsymbol{m}/\partial t\}^n \tag{3b}$$

如果在特定时刻所有的场分量都可以获得，那么上面有限差分近似的引入误差为 $O\lfloor(\Delta t)^2\rfloor$。在指定的 n 时刻，计算 $\boldsymbol{m}$ 的偏导需用到 $\boldsymbol{h}^n$。为方便起见，设 $\boldsymbol{H}_0=0$，$\boldsymbol{M}_0=M_0\hat{y}$，则式 (2c) 变为

$$\{\partial\boldsymbol{m}/\partial t\}^n=-\gamma\boldsymbol{M}_0\times\boldsymbol{h}^n \tag{4}$$

不幸的是，$\boldsymbol{h}^n$ 并不能直接得到。简单办法是设 $\boldsymbol{h}^n=\boldsymbol{h}^{n-1/2}$，但只能保证差分精度 $O[\Delta t/2]$。如果采用 (5) 式的外插式去满足 (4) 式对时间的苛求，我们可以获得更高的精度。

$$\boldsymbol{h}^n\approx\boldsymbol{h}^{n-1}+\{\partial\boldsymbol{h}/\partial t\}^{n-1}\Delta t=(1/2)(3\boldsymbol{h}^{n-1/2}-\boldsymbol{h}^{n-3/2}) \tag{5}$$

相应地，$\boldsymbol{m}$ 的时间偏导近似式可写为

$$\{\partial\boldsymbol{m}/\partial t\}^n\approx-(\gamma/2)\boldsymbol{M}_0\times(3\boldsymbol{h}^{n-1/2}-\boldsymbol{h}^{n-3/2}) \tag{6}$$

则可以导出式 (2b) 中 $h_x^{n+1/2}$ 和 $h_z^{n+1/2}$ 的差分式如下：

$$h_x^{n+1/2}=h_x^{n-1/2}-(\Delta t/\mu_0)\hat{x}\cdot\{\nabla\times\boldsymbol{E}\}^n+s(3h_z^{n-1/2}-h_z^{n-3/2}) \tag{7}$$

$$h_z^{n+1/2}=h_z^{n-1/2}-(\Delta t/\mu_0)\hat{z}\cdot\{\nabla\times\boldsymbol{E}\}^n+s(3h_x^{n-1/2}-h_x^{n-3/2}) \tag{8}$$

其中 $s=\Delta t(\gamma M_0/2)$，上两式是非耦合的并且可以方便地导出 FDTD 迭代方程。如果 $\boldsymbol{H}_0\neq0$，直接计算场量 $\boldsymbol{h}$ 已不可能。这时，必须先计算出磁化强度 $\boldsymbol{m}$，然后将它的时间偏导用于 $\boldsymbol{h}$ 场的迭代。对 y 方向的外加偏置磁场其迭代方程如下：

$$m_x^{n+1/2}=m_x^{n-1/2}+(\Delta t/2)\gamma[H_0(3m_z^{n-1/2}-m_z^{n-3/2})-M_0(3h_z^{n-1/2}-h_z^{n-3/2})] \tag{9}$$

$$m_z^{n+1/2}=m_z^{n-1/2}-(\Delta t/2)\gamma[H_0(3m_x^{n-1/2}-m_x^{n-3/2})-M_0(3h_x^{n-1/2}-h_x^{n-3/2})] \tag{10}$$

$$h_x^{n+1/2}=h_x^{n-1/2}-(\Delta t/\mu_0)\hat{x}\cdot\{\nabla\times\boldsymbol{E}\}^n-(m_x^{n+1/2}-m_x^{n-1/2}) \tag{11}$$

$$h_z^{n+1/2}=h_z^{n-1/2}-(\Delta t/\mu_0)\hat{z}\cdot\{\nabla\times\boldsymbol{E}\}^n-(m_z^{n+1/2}-m_z^{n-1/2}) \tag{12}$$

用与上述相同的步骤不难推出外加偏置磁场为任意方向的通用差分式。

从 (9) 式与 (10) 式可以看出，计算 m_x 时要用到 m_z 和 h_z，而在 Yee 氏网格中，虽然 m_z 和 h_z 空间位置相同，但 m_x 和 m_z 空间位置不同，为了消除这种空间上的错位，我们使用了内插方法。以图 1 所示的二维 FDTD 网格为例，在 m_x 处的 m_z 近似为

$$m_{zi}(i,j+1/2)\approx(1/2)[m_z(i-1/2,j+1/2)+m_z(i+1/2,j+1/2)] \tag{13}$$

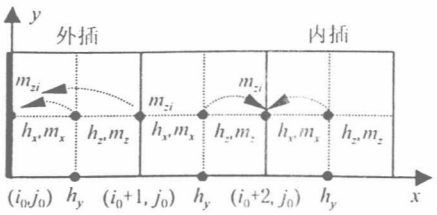

图 1 Yee 氏网格中的内插和外插表

下标 i 表示内插值. 在材料的边界处, 上述内插表将被破坏, 这时要用外插法来代替. 如在点 $i=i_0, j=j_0$ 处有

$$m_{zi}(i_0, j_0+1/2) \approx 2m_z(i_0+1/2, j_0+1/2) - m_{zi}(i_0+1, j_0+1/2)] \tag{14}$$

将插值 $m_{\eta i}$ 代替 (9) 式与 (10) 式右边的 $m_\eta(\eta$ 为 $x,y,z)$ 并对 h_η 作同样处理就可以实现空间上的同步.

2.2 激励源的类型和设置

研究微带天线的 RCS 频响特性, 使用高斯脉冲平面波作为激励源是方便的. 其函数形式为

$$E_i(t) = \exp[-(t-t_0)^2/T^2] \tag{15}$$

对 (15) 式做傅里叶变换得

$$|E_i(f)| = T\sqrt{\pi}\exp(-\pi^2 T^2 f^2) \tag{16}$$

计算中取 $T=0.5/f_h$, f_h 的选择略大于所需考察频段的最高频率, 另外考虑到源的初始条件 $E_i(t=0)\to 0$ 取 $t_0=4T$. 为了在 FDTD 运算过程中“提取”出散射场, 将计算域划分成总场区和散射场区 [9] , 激励源设置在总场区和散射场区的连接面上.

2.3 吸收边界条件

用 FDTD 求解电磁散射问题时, 由于计算机内存限制我们必须将网格界定在一个有限区域内. 为了达到模拟无限区域的目的, 必须引入吸收边界条件以减小非物理原因导致的反射. 本文采用了 B. Chen 和 D. G. Fang 在 J. P. Berenger 完全匹配层 (PML)[10] 基础上改进的完全匹配层 (MPML)[11] .

2.4 雷达截面

三维散射体的雷达截面定义为

$$\sigma = 4\pi R^2 \lim_{R\to\infty} |E_s/E_i|^2 \tag{17}$$

式中 R 是坐标原点到观察点间的距离, E_i 是入射平面波电场分量, E_s 是散射波在观察点的电场分量. 用 FDTD 法分析时, 得到的只是散射体附近的近区散射场. 本文运用 R. J. Luebers 提出的时域近场–远场变换方法 [12] 由近区散射场计算出远区散射场值.

3 数值结果

图 2 所示的是图 3 铁氧体矩形微带贴片天线在不同方向的外加偏置磁场作用下 $\sigma_{\theta\theta}$ 的频响特性曲线, 图中同时给出了未加偏置磁场的矩形微带贴片天线的 RCS . 射频场显示表明辐射的口径场主要集中在辐射边附近很小的区域内, 介质的过多向外延伸对这种场分布没有明显影

响，实验表明沿辐射元各边向外延伸 $\lambda_g/10$ 就可以了[13]，λ_g 为微带天线中最低模式的工作波长，它由腔模理论直接求得。基于上述理由，这里基片尺寸取为

$$L_xG = L_x + 0.2\lambda_g, \quad L_yG = L_y + 0.2\lambda_g \tag{18}$$

天线的其它参数为 $L_x = 0.55$cm，L_y=0.4cm，d=0.06cm，ε_r=12.8，$M_0 = 1780$G，$H_0 = 360$Oe。计算域的设置如图 4 所示。计算中取 $\theta = 60°$，$\varphi = 45°$，$\Delta = 0.2$mm，$d_x = 1.0185$，$d_y = d_z = 1.0$，总场网格数为 151×144×8，散射场区厚度为 5 格，吸收层厚度为 8 格。考虑到微带天线是高 Q 谐振结构，迭代收敛缓慢，根据经验计算总时间步数取为 32768。

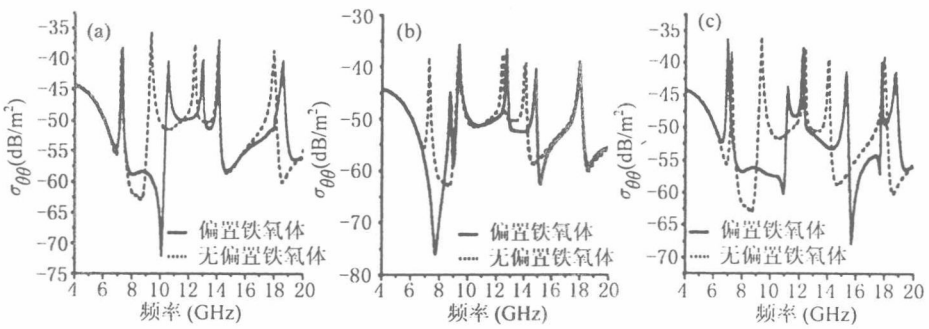

图 2　不同方向偏置磁场情况
(a) y 方向　(b) x 方向　(c) z 方向

由图 2(a) 知，沿 y 方向外加偏置磁场不影响天线的第一个谐振频率点位置。这是因为在未加偏置磁场时，第 1 谐振频率对应腔模中的 TM_{10} 模，而在 TM_{10} 模中，H_x 和 H_z 与 H_y 相比可以忽略，E_x 和 E_y 与 E_z 相比也可以忽略。从 Maxwell 方程可知，H_y 和 E_z 几乎不受外加偏置磁场影响。由于该天线的第 4 个谐振频率对应 TM_{20} 模，基于同样的原因也不受外加偏置磁场影响。另外一些谐振点发生了频率偏移但 RCS 大小几乎不变。由图 2(b) 知，与 y 方向外加偏置磁场讨论相似，沿 x 方向外加偏置磁场对 TM_{0n} 模影响很小。第 2、5 谐振频率就属于这种情况，它们分别对应 TM_{01} 模和 TM_{02} 模。从图上还可看出第 1 谐振频率增加了 1.2GHz 并且第 1、2 谐振频率变得很靠近 (0.6GHz)。由图 2(c) 知，当外加 z 方向偏置磁场时，第 1 谐振频率减小而第 2 谐振频率增加，从而两个谐振频率间距大大增加。上述结论与文献 [3] 完全吻合。计算曲线与文献 [3] 中图 2, 3, 4 比较，在第 1 谐振频率以下误差较大，其原因有：(1) 计算模型上的差异；(2) 受计算机资源限制，计算域和总时间步还不足够地大。

图 5 给出了 $\sigma_{\theta\phi}$ 的频响特性曲线。从图中可以看出，外加偏置磁场对谐振频率偏移的效果与同极化时相同。

对于图 3 的铁氧体微带贴片天线，在未加偏置磁场的情况下，还探讨了有限接地平面和宽基片对天线 RCS 频响特性的影响。图 6 给出了 1.01cm×0.86cm 有限接地平面情况下天线的 RCS 频响特性曲线，计算中取 $\theta = 60°$, $\varphi = 45°$, $\Delta = 0.1$mm, $d_x = d_y = d_z = 1.0$, 总场网格数为 $111 \times 96 \times 16$, 散射场区厚度为 5 格，吸收层厚度为 8 格。结果表明有限接地平面会使天线的 RCS 谐振特性变差，并且整体下降若干分贝；若基片很大，可以将基片插入到吸收层中。计算中取 $\theta = 60°$, $\varphi = 45°$, $\Delta = 0.2$mm, $d_x = d_y = 2.5$, $d_z = 1.0$, 总场网格数为 $101 \times 86 \times 8$, 散射

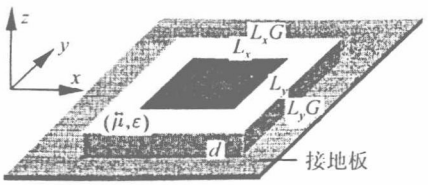

图 3 铁氧体矩形微带贴片天线

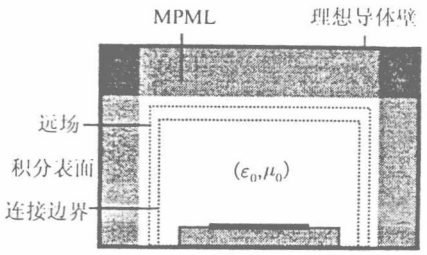

图 4 微带天线的 FDTD 计算域设置

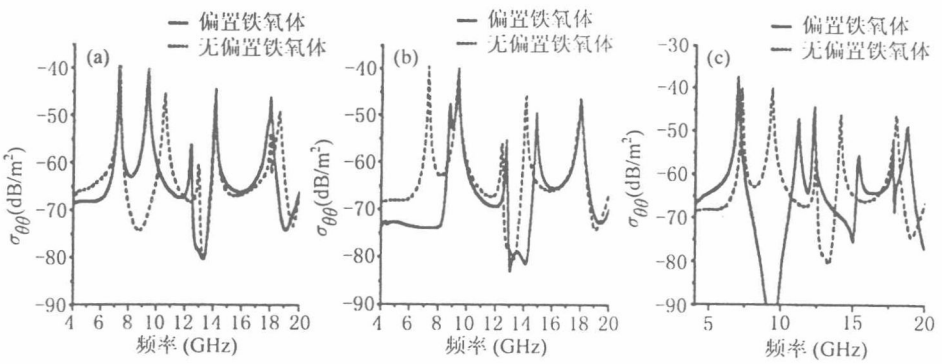

图 5 不同方向偏置磁场情况
(a) y 方向 (b) x 方向 (c) z 方向

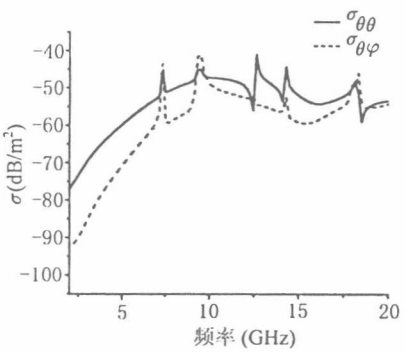

图 6 有限接地板微带天线的 RCS

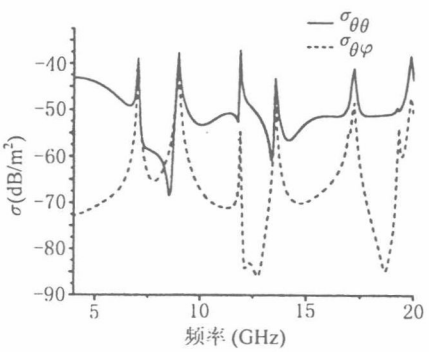

图 7 宽基片微带天线的 RCS

场区厚度为 5 格，吸收层厚度为 16 格．计算结果见图 7，可以看出基片在长度和宽度方向的延伸对微带天线的 RCS 影响很小．

4 结 论

本文在 FDTD 法分析研究铁氧体微带天线的 RCS 频响特性中，通过铁氧体进动方程，绕过了铁氧体色散媒质所导致的时域卷积而给 FDTD 法应用带来的困难．与谱域矩量法相比，本

文 FDTD 法推导过程简单，应用方便灵活，既适用于任意方向的外加偏置磁场，又适用于多层铁氧体加载的结构形式。

参 考 文 献

[1] D. M. Pozar, V. Sanchez, Magnetic tuning of a microstrip antenna on a ferrite substrate, Electron. Lett., 1988, 24(12), 729–731.

[2] P. J. Rainville, F. J. Harackiewicz, Magnetic tuning of a microstrip patch antenna fabricated on a ferrite film, IEEE Microwave and Guided Wave Lett., 1992, 2(12), 483–485.

[3] H. Y. Yang, J. A. Castaneda, N. G. Alexopoulos, The RCS of a microstrip patch on an arbitrarily biased ferrite substrate, IEEE Trans. on AP, 1993, 41(12), 1610–1614.

[4] B. Lee, F. J. Harackiewicz, The RCS of a microstrip antenna on an In-Plane biased ferrite substrate, IEEE Trans. on AP, 1996, 44(2), 208–211.

[5] G. Zheng, K. Chen., Transient analysis of microstrip lines with ferrite substrate by extended FD-TD method, Int. J. Infrared & Millimeter Waves, 1992, 13(8), 1115–1124.

[6] A. Reinex, T. Monediere, E. Jecho, Ferrite analysis using the finite-difference time-domain(FDTD) method, Microwave and Opt. Tech. Lett., 1993, 5(13), 685–686.

[7] J. A. Pereda, *et al.*, A treatment of magnetized ferrites using the FDTD method, IEEE Microwave and Guided Wave Lett., 1993, 3(5), 136–138.

[8] M. Okoniewski, E. Okoniewska, FDTD analysis of magnetized ferrites: A more efficient algorithm, IEEE Microwave and Guided Wave Lett., 1994, 4(6), 169–171.

[9] K. R. Umashankar, A. A. Taflove, Novel method to analyze electromagnetic scattering of complex objects. IEEE Trans. on EMC, 1982, 24(4), 397–405.

[10] J. P. Berenger, A perfectly matched layer for the absorption of electromagnetic waves , J. of Computational Physics, 1994, 114(2), 185–200.

[11] B. Chen, D. G. Fang, B. H. Zhou, Modified Berenger PML absorbing boundary condition for FD-TD meshes, IEEE Microwave and Guided Wave Lett., 1995, 5(11), 399–401.

[12] R. J. Luebers, K. Kunz, M. A. Schneider, Finite-difference time-domain near zone to far zone transformation, IEEE Trans. on AP, 1991, 39(4), 429–433.

[13] 张均，刘克诚，张贤铎，赫崇骏，微带天线理论与工程，北京，国防工业出版社，1988, 117–118.

THE RCS OF A MICROSTRIP ANTENNA ON AN ARBITRARILY BIASED FERRITE SUBSTRATE USING FDTD

Xin Yaming　　Gu Changqing

(*Nanjing University of Aeronautics and Astronautics, Nanjing* 210016, *China*)

Abstract　In this paper, a more efficient FDTD algorithm, with the Gilbert's equation of motion being discretized directly, is introduced for the analysis of the RCS of a microstrip patch on an arbitrarily biased ferrite substrate. Some new techniques are adopted. Numerical examples are given.

Key words　Microstrip antenna, FDTD, RCS, Ferrite

辛雅明：　男，1974 年生，硕士生，感兴趣研究方向为天线与电磁兼容.

顾长青：　男，1958 年生，教授，主要研究方向为天线、电磁散射和电磁兼容.

An Efficient Topography Adaptive Filter for Insar Processing*

Zhu Daiyin(朱岱寅), Scheiber Rolf**, Sha Nansheng***, Zhu Zhaoda
(Department of Electronic Engineering, Nanjing University of Aeronautics and Astronautics, Nanjing 210016, P.R.China)
(** Deutsches Zentrum für Luft- und Raumfahrt (DLR) e.V.)
(*** Department of Automatic Control, Beijing University of Aeronautics and Astronautics, Beijing 100083, P.R.China)

Abstract

An efficient implementation of the topography adaptive filter based on local frequency estimation is proposed, where chirp-z transform is applied to enhance the accuracy of the frequency estimation. As a by-product of this adaptive filter, the linear approximated phase model of the interferogram is employed to improve the coherence estimation. The impacts of the adaptive filter on global and local phase unwrapping algorithms are discussed. Finally, aiming at the negative effect that the adaptive filter can bring to local phase unwrapping algorithms, a fusion scheme that takes advantage of least square and several local phase unwrapping algorithms is presented.

Key words: Interferometric SAR, Local frequency estimation, Chirp-z transform, Phase unwrapping

0 Introduction

Interferometric SAR (InSAR) is powerful in digital topography modeling, even though, the thermal noise, spatial and temporal decorrelation noise, which make the interferogram quite noisy, always encumber us from deriving as much as possible the terrain characteristic from the two complex SAR images acquired from different orbits. To filter the interferogram is one of the crucial steps in the InSAR signal processing routine, without which it is almost impossible to unwrap the phase correctly, and hence to reconstruct the topography. The purpose of the filtering of the interferogram is to reduce the phase noise and "repair" phase fringes. The interferometric phase that has been wrapped into the interval of $[-\pi, +\pi]$ should be considered as a random process, and is supposed to be stationary in a small area although it is not true in the large extent of the interferogram. To filter the interferogram with a moving box is called "multilook", it is the maximum likelihood estimator of the interferometric phase originating from constant terrain after the flat earth phase is removed. With an appropriate number of "looks", we can reduce the phase noise, and improve the contrast of the interferometric phase map as well. The so-called "multilook filter" is essentially a 2-D low pass filter, it eliminates the signal in case of steep topography as well as suppresses noise in the stop band. So, the multilook filter will smear the tight fringes of the interferometric phase map, and also cause underestimation at the precipitous terrain. We try to overcome this defect of the multilook filter by a local frequency estimation technique, which will center the pass band of the 2-D filter on the maximum magnitude of the 2-D local Fourier spectrum of the interferogram. Local frequency estimation makes the pass-band of the filter track the variation of the topography, in other words, it introduces a topography adaptive filter.

In the recent literature, there are diverse schemes to implement the filtering of the interferogram by local frequency estimation techniques. For example, the schemes in Ref.[1-3] are based on the MUSIC algorithm, 2-D FFT, and Energy Separation Algorithm, respectively. In this paper, we propose a chirp-z based scheme in Section 1. During the implementation of the filtering scheme the linear approximated phase model of the interferogram is extracted as a by-product, which can help to improve the coherence estimation, and hence provide a more reasonable quality map for phase unwrapping. In section 2 and 3, the impacts brought by this topography adaptive filter on coherence estimation and phase unwrapping algorithms are analyzed respectively. To remove the negative effect caused by this adaptive filter on the local phase unwrapping algorithms, in section 4, a phase unwrapping scheme based on the fusion of the least square and several local phase unwrapping algorithms is proposed. We use X-SAR data of the Mt. Etna and ERS data taken from the vicinity of Vienna as examples to study the performance of the filter.

* Supported by the National Natural Science Foundation of China.
Received May 9, 2001

1 The Topography Adaptive Filter

Two complex SAR images used for interferometry can be modeled as,

$$\begin{aligned} s_1 &= c + n_1 \\ s_2 &= c \cdot e^{-j\phi_T} + n_2 \end{aligned} \tag{1}$$

Here, c is the common part in the two SAR images, n_1 and n_1 are the decorrelation noise,, and are assumed to be uncorrelated circular Gaussian random processes, and ϕ_T is the phase caused by the topography. We use the conjugate multiplication to form the interferogram,

$$\begin{aligned} I = {} & |c|^2 \cdot e^{j\phi_T} + c \cdot n_2^* + c^* \cdot n_1 \\ & \cdot e^{j\phi_T} + n_1 \cdot n_2^* \end{aligned} \tag{2}$$

I is non-stationary because of the term $|c|^2 \cdot e^{j\phi_T}$, whereas the remaining three terms are stationary in a wide sense. Strictly speaking, it is not reasonable to do moving average over the interferogram because of its non-stationarity, especially in conditions that the terrain is very precipitous. In such areas, even the rough assumption, that I is stationary in a small window is no longer correct, and the moving average that ignores this point will smear the fringes. The first term of (2) can be decomposed as:

$$e^{j\phi_T} \cdot |c|^2 \cdot e^{j(\phi_T - \phi_r)} \tag{3}$$

where ϕ_r is the coarse topography phase, and $|c|^2 \cdot e^{j(\phi_T - \phi_r)}$ stands for the detail of the topography. If we are able to extract the coarse topography phase from the interferogram, then (2) is rewritten as,

$$\begin{aligned} I = {} & e^{j\phi_r} \cdot [|c|^2 \cdot e^{j(\phi_T - \phi_r)} + c \cdot n_2^* \cdot e^{-j\phi_r} \\ & + c^* \cdot n_1 \cdot e^{j(\phi_T - \phi_r)} + n_1 \cdot n_2^* \cdot e^{-j\phi_r}] \end{aligned} \tag{4}$$

The detail of the topography, i.e. the term $|c|^2 \cdot e^{j(\phi_T - \phi_r)}$ is the mean of the stationary process in the brackets of (4). We can achieve the maximum likelihood estimation (MLE) of it by moving average under the assumption of ergodicity. The extraction of the coarse topography can be accomplished by fringe detection. In our filtering scheme, this goal is achieved by generating a linear approximated interferometric phase model.

1.1 *Structure of the Topography Adaptive Filter*

The topography adaptive filter is a linear system, and it should be expressed in the spatial domain as,

$$\{[I(j,k) \cdot h_{\text{estimated fringe}}(j,k))^*] \otimes h_{\text{moving box}}(j,k)\} \cdot h_{\text{estimated fringe}}(j,k) \tag{5}$$

where $h_{\text{moving bxo}}(j,k)$ is the impulse response function of a moving boxcar filter, and $h_{\text{estimated fringe}}(j,k)$ is the estimated linear phase model, which stands for the coarse topography phase. $\otimes$ denotes the two dimensional convolution. The term $h_{\text{estimated fringe}}(j,k)$ plays the key role in the above filter, and is determined by the input interferogram through local fringe detection. If interpreted from the viewpoint of a band pass filter, it is the linear approximated phase model that provides information on the location of the center of the local interferogram spectrum, and hence guides us to design the band pass filter.

1.2 *Implementation of the Filter*

The most noticeable feature of the interferometric phase map is its fringe pattern. If we separate a fairly small part of this interferogram, it should be possible to approximate its phase map with a plane. The spatial frequency of this two-dimensional linear phase can be estimated from the small separated interferogram by several methods. While estimating the frequency with 2-D FFT, the spectrum must be interpolated to improve the accuracy of the estimation. Computational complexity will be reduced if we only make interpolation in the main lobe of the spectrum. A 2-D FFT of the original size on the separated interferogram will bring us a coarse spectrum, then after its main lobe is located, only interpolation within this main lobe is needed to get a precise estimation of the local frequency. Chirp-z transform, which allows us to only achieve very high frequency sampling rate in a small interval on the unit circle, is employed to compute the discrete Fourier Transform within a small frequency interval[4].

The estimated phase plane is described as:

$$\phi(f_j, f_k) = e^{j2\pi(f_j \cdot j + f_k \cdot k)} \cdot e^{j\phi_o} \tag{6}$$

where f_j, f_k are the maximum likelihood estimates of the 2-D spatial frequency components, and ϕ_o is the initial phase. $e^{j\phi_o}$ is computed as the normalized complex average of the separated interferogram after the linear phase is removed from it.

At the same time that we get the coarse 2-D Fourier spectrum of a separated interferogram, the local SNR can be evaluated by the ratio between the magnitudes of the main lobe and side lobe of the spectrum. The local SNR is also a scale of the confidence of the frequency estimation. If the local SNR is smaller than a given threshold, we enlarge the estimation window to twice of its original size for more reliable estimation results and calculate the local SNR again. If the new SNR is still lower than the threshold, a mandatory spatial frequency of 0 is set. The mandato-

ry frequency is usually assigned to areas that are totally decorrelated (e. g. water, high vegetation in repeat-pass InSAR).

We go through the whole interferogram by 50 percent overlapping the estimation window, then taper weighting the estimated 2-D linear phasor, after that reassembling them by superposition[5] to get $h_{\text{estimated fringe}}(j, k)$, i. e. the linear approximated phase model. Because the computational efficiency of making maximum likelihood estimation on the phase of each pixel is not acceptable, the overlapping can also be considered as an interpolation scheme, which avoids estimating the dominant 2-D frequency point by point over the whole map. An example of the performance of this filtering scheme is presented in Fig. 1. The input interferometric phase and the linear approximated phase model extracted from X-SAR Mt. Etna data are shown in Fig. 1(a) and Fig. 1(b) respectively.

The local SNRs will also be combined after taper weighting to get an SNR map of the interferogram, which can also be used as an additional quality map for phase unwrapping.

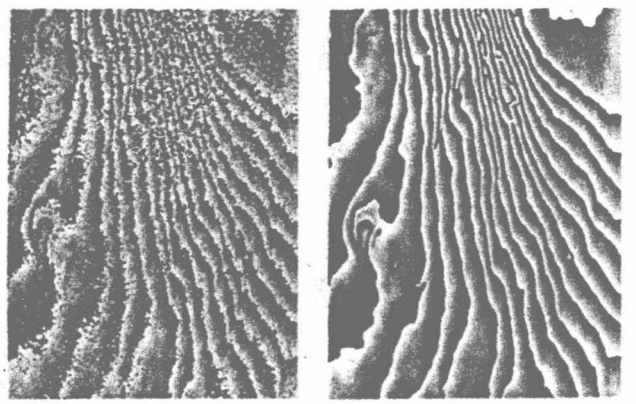

(a) (b)

Fig. 1 Interferometric phase (a) and linear approximated phase model (b) of X-SAR Mt. Etna data

2 Impacts of the Linear Phase Model on Conherence Estimation

We improve the coherence estimation by identifying the topography term with the linear approximated phase model $h_{\text{estimated fringe}}$. It should be removed from the interferogram prior to the estimation of the coherence over a large window. Thus the product of thermal and temporal decorrelation $\gamma_{\text{thermal}} \cdot \gamma_{\text{temporal}}$ should be estimated as,

$$\gamma_{\text{thermal}} \cdot \gamma_{\text{temporal}} = \frac{\left| \sum_{j,k \in w} s_1 \cdot s_2^* \cdot h^*_{\text{estimated fringe}} \right|}{\sqrt{\sum_{j,k \in w} |s_1|^2 \cdot \sum_{j,k \in w} |s_2|^2}} \quad (7)$$

Additionally, the linear approximated phase mode can also be used for the spatially adaptive implementation of the spectral shift filter as proposed in Ref. [6].

3 Impacts of the Adaptive Filter on Phase Unwrapping

The performance of the filtering scheme should be investigated with respect to its impacts on phase unwrapping. In general the adaptive filter should facilitate phase unwrapping, but sometimes it also has negative effects because of the artificial fringes caused by the noise corrupted frequency estimation. In this section, we will study the impacts of the adaptive filter on the global and local phase unwrapping algorithms and put emphasis on the negative effect in the case of local methods from the perspective of residue distribution.

3.1 *Impacts on the Least Square Phase Unwrapping Method*

As is well known[7], phase noise induces slope under estimation for least square phase unwrapping algorithms. Therefore filtering must be proceeded prior to least square phase unwrapping methods. It is well known[1-3] that a topography adaptive filter performs better than the conventional multilook filter. Nevertheless, the need for weighting/masking particular areas cannot in general be overcome. The generation of the adequate weights is not necessarily solved by the proposed topography adaptive filter, but the performance of least square methods is generally improved.

3.2 *Impacts on the Local Phase Unwrapping Methods*

If the phase unwrapping problem is not singular there is definitely a reasonable or correct way to define the integral path for local phase unwrapping methods along which unwrapping errors will be localized. Nevertheless, our capability of defining it is problematic in case of high residue density the correct way is usually unavailable and the robustness of any of the local algorithms will be destroyed due to the high level of phase noise.

To compensate the shortness of our ability to find the right integral path in noisy phase maps, filtering of the interferogram is still necessary as a preprocessing step of local algorithms. Despite that the topography adaptive filter can greatly reduce the residue density, sometimes it also has negative effect on the local algorithms. This is caused by the artificial fringes generated by the filter in the situation of low coherence. The artificial fringes that make difficulties for phase unwrapping do not come from topography, b

from noise.

For some certain residue distributions like dipoles and near distance residue pairs it is very easy to define a reasonable integral path, while for isolated residues it becomes quite difficult. From the perspective of residue distribution, the artificial fringes generated by the local frequency estimator in low coherence areas often bring us residue pairs with farther distance and even isolated residues. Artificial fringes do not tend to make the phase unwrapping problem singular, but as the distance between residues is enlarged, to connect residues with opposite charges sometimes does become more difficult.

The linear approximated phase model $h_{\text{estimated fringe}}(j,k)$ in the filtering scheme is normally not rotation free. After it has been subtracted from the input interferogram, the residue map of the residual phase, which is expressed as the principal phase value of the term in the brackets of Equation (4) must be different from that of the input interferogram. The residue pairs with farther distance and isolated residues caused by artificial fringes will also appear in the residue map of the residual phase. The residual phase will be multilooked afterwards, but the adverse residue distribution can still remain even after being smoothed. Next, to finish the filtering process, the smoothed residual phase has to be added back to the linear approximated phase model. In this step, two phase maps both with artificial residues, will be superimposed to each other and there is no guarantee that these artificial residues will cancel out or form near distance residue pairs. To overcome these problems we propose the following fusion scheme.

4 A Fusion Scheme for Phase Unwrapping

In order to adapt the filtering scheme to path following methods, we propose a modified version of the adaptive filter. As is well known, least square methods can give a smooth result, so our intention is to modify $h_{\text{estimated fringe}}(j,k)$ through unwrapping it with the unweighted least square estimator. In this way, usually a residue free phase field can be obtained. After subtracting it from the input interferogram we get a residual phase map, which has nearly the same residue distribution as the input interferogram. To unwrap the residual phase map by any path following method is as difficult or as easy as to directly unwrap the phase map of the input interferogram because of the same residue map they have. Before smoothing the residual phase to reduce the phase noise, the artificial residues do not occur and after the smoothed residual phase is added back to the unwrapped linear approximated phase model, still no artificial residues are introduced.

Our fusion scheme for phase unwrapping is described next: First the modified adaptive filtering scheme is proceeded; Then for phase unwrapping, we first generate the mask cuts with the mask cut algorithm[8], and then unwrap the smoothed residual phase. During the unwrapping process a binary map is generated, which is a flag on each pixel and indicates if it has been unwrapped or not. Then the areas marked as wrapped are unwrapped with a region growing algorithm. For the region growing algorithm, pseudo-correlation is utilized as a quality map. Pseudo-correlation can point out the position of residues very precisely, and the integral path of region growing will be guided in a more appropriate manner. Besides the pseudo-correlation, the SNR map is also used to set a lower limit to stop the region growing. The reason why two different quality maps are used here is just for the improvement of the robustness. An example of phase unwrapping using the fusion scheme is presented in Fig. 2.

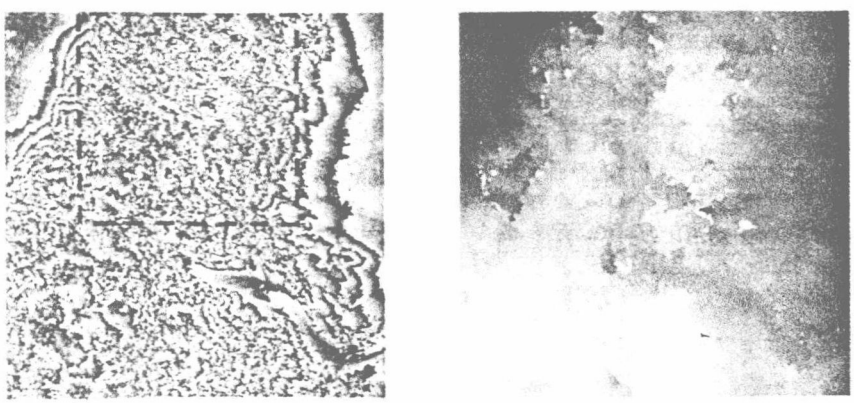

(a) Wrapped phase map (b) Unwrapped phase

Fig. 2 Results of phase unwrapping using the fusion scheme

5 Summary

An efficient implementation of the topography adaptive filter based on the chirp-z transform has been presented. Its potential to repair fringes was shown, but sometimes it also induces broken or lost fringes because of the artificial fringes caused by the corrupted frequency estimation. Therefore the adaptive filter incorporated with the least square estimator is suggested prior to using the local phase unwrapping algorithms.

Acknowledgement: The work presented in this paper was performed within a collaboration of the Chinese Aeronautical Establishment (CAE) and the German Aerospace Center (DLR).

References

[1] Trouve E, Nicolas J, Maitre H. *IEEE Trans Geosci Remote Sensing*, 1998, 36(11): 1963

[2] Hubig M. A maximum likelihood a priori filter for interferometric phase. In: Proceedings of IGARSS'99, 1999

[3] Perea-Vega D, Cumming I. Local frequency estimation in interferograms using a multiband pre-filtering approach. ESA-Fringe Workshop'99, 1999

[4] Oppenheim A V, Schafer R W. Discrete Time Signal Analysis. London: Prentice Hall, 1999

[5] Goldstein R, Werner C. Radar ice motion interferometry. In: Proc. 3rd ERS Symp. on Space at the Service of Our Environment, Florence, Italy: Mar. 1997

[6] Davidson G W, Bamler R. *IEEE Trans Geosci Remote Sensing*, 1999, 37(1): 163

[7] Bamler R, Adam N, Davidson G W, et al. *IEEE Trans Geosci Remote Sensing*, 1998, 36(5): 913

[8] Flynn J. Consistent 2-D phase unwrapping guided by a quality map. In: Proceedings of IGARSS'96, 1996

Zhu Daiyin, born in 1974, received his B.S. degree from the Department of Radio Engineering, Southeast University, Nanjing, and his M.S. degree from the Department of Electronic Engineering, Nanjing University of Aeronautics and Astronautics(NUAA) in 1996 and 1998, respectively. He is now working towards Ph.D. degree in NUAA. His research interests include radar imaging and signal processing.

机载 SAR 斜视区域成像研究

朱岱寅[1],朱兆达[1],叶少华[2],张昆辉[2],谢求成[1]
(1. 南京航空航天大学电子工程系,江苏南京 210016;2. 雷华电子技术研究所,江苏无锡 214063)

摘 要: 本文研究机载合成孔径雷达(SAR)斜视区域成像,提出在一维距离像上对地面像素逐个进行距离对准和相位补偿的运动补偿方法.该方法在完成斜地校正的同时,还能有效地改善方位聚焦并减小几何失真.用上述运动补偿方法和线性 R-D 成像算法,某型机载 SAR 在试飞实验中成功实现了斜视区域成像.

关键词: 机载 SAR; 斜视; 区域成像; 运动补偿
中图分类号: TN957 **文献标识码:** A **文章编号:** 0372-2112 (2002) 09-1387-03

Studies on Airborne Squint-Looking SAR Patch-Mapping

ZHU Dai-yin[1], ZHU Zhao-da[1], YE Shao-hua[2], ZHANG Kun-hui[2], XIE Qiu-cheng[1]
(1. *Department of Electronic Engineering, Nanjing University of Aeronautics and Astronautics, Nanjing, Jiangsu* 210016, *China*;
2. *Chinese Leihua Electronic Technology Research Institute, Wuxi, Jiangsu* 214063, *China*)

Abstract: The operation and processing of airborne squint-looking SAR patch-mapping is investigated. For motion compensation, we propose to perform the range alignment and phase compensation on the one-dimensional range profile in a pixel by pixel level. By the simulation, we can see that compared with the simple method that does motion compensation only according to the center of the illuminated area, the new motion compensation method not only can improve azimuthal focusing and reduce geometric distortion, but also may simultaneously realize ground projection. With the linear R-D algorithm and the proposed motion compensation method, airborne squint-looking SAR patch-mapping has been implemented successfully in a campaign. And an X-band SAR image of mountainous area of 40 degree squint angle is presented at the end of this paper.

Key words: airborne SAR; squint-looking; patch-mapping; motion compensation

1 引言

斜视区域成像是机载合成孔径雷达(SAR)的重要成像模式,对军用机载 SAR 尤为重要[1,2].同机载 SAR 的任何模式一样,运动补偿是成像的前提.

在斜视区域成像中,通过运动补偿消除成像区相对于载机的平动对回波信号时延的影响,只保留成像区相对于其中心的转动分量.一般做法是从回波信号中去除与成像区中心点对应的时延值[3,4].具体讲,在直接距离脉压方式中,运动补偿分为距离对准和相位补偿二个步骤.运动补偿所需要的成像区中心点时延值,由雷达天线相位中心到成像区中心的距离决定,该距离根据机上 IMU/GPS 提供的信息来计算.

我们在研究中发现,从回波信号去除成像区中心点时延的方法会引起图像的失真;另外,还需要通过斜地校正才能得到地面图像.本文提出一种运动补偿方案,对一维距离像按照地面像素位置进行重新抽样,同时完成距离对准和相位补偿;这样可以有效改善方位聚焦和降低图像几何失真,并同时实现了斜地校正.

本文第二节给出 SAR 斜视区域成像的几何关系.第三、四节介绍在一维距离像上对地面像素逐个进行校正的运动补偿方法.其中第三节叙述距离对准,第四节叙述相位补偿.第五节介绍某型机载 SAR 试飞实验成像结果.第六节为简短结论.

2 几何关系

图 1 是考虑载机飞行高度时,斜视成像模式的几何关系示意图.按右手准则建立三维坐标系,地面成像区处于 xy 平面上,如图阴影部分所示.理想情况下载机以速度 V_a 沿水平直线飞行,合成孔径起点为 A,终点为 B,AB 平行于 x 轴,线段 AB 对成像区中心点的张角为 $\Delta\theta$.P 是 AB 的中点.飞行高度 $H = PQ$,PO(即天线指向)与载机前进速度的夹角为 α,α 在地面投影为 β.雷达成像距离 $R = PO$.

实际飞行中,飞机将偏离匀速直线运动,在任一时刻 t,其位置坐标($x(t)$,$y(t)$,$z(t)$)由 IMU/GPS 提供.

收稿日期:2001-06-28;修回日期:2001-12-20
基金项目:国家自然科学基金(No.60082002);国家 863 计划(No.863-308-11-03(1))